Spark Plasma Sintering, Mechanical and *In-vitro* Behavior of a Novel Sr- and Mg-Containing Bioactive Glass for Biomedical Applications

Damiano Angioni[1], Roberto Orrù[1,*], Giacomo Cao[1], Sebastiano Garroni[2], Antonio Iacomini, Devis Bellucci[3], Valeria Cannillo[3]

[1]*Dipartimento di Ingegneria Meccanica, Chimica e dei Materiali, Unità di Ricerca del Consorzio Interuniversitario Nazionale per la Scienza e Tecnologia dei Materiali (INSTM), Università degli Studi di Cagliari, via Marengo 2, 09123 Cagliari, Italy*

[2]*Dipartimento di Chimica e Farmacia, Università degli Studi di Sassari, Via Vienna 2, 07100 Sassari, Italy*

[3]*Dipartimento di Ingegneria "Enzo Ferrari", Università degli Studi di Modena e Reggio Emilia, Via P. Vivarelli 10, 41125 Modena, Italy*

* Author to whom correspondence should be addressed:

R. Orrù (E-mail: roberto.orru@dimcm.unica.it; Ph.: +39-070-6755076; Fax: +39-070-6755057), *Università degli Studi di Cagliari, via Marengo 2, 09123 Cagliari, Italy*

https://doi.org/10.1016/j.jeurceramsoc.2021.11.061

Abstract

The so-called BGMS10, a bioactive glass containing 10 mol.% SrO and 10 mol.% MgO, displays a low inclination to crystallize, as confirmed by its high activation energy (538.9 kJ/mol). Such peculiar aspect and the beneficial use of SPS allow for the obtainment of 99.7 % dense and fully amorphous products at 750°C. The incipient crystallization in the glass is induced when temperature is increased to 850°C, while 95 wt. % crystallized ceramics are produced at 950°C. Crystalline phases detected are α- and β-$CaSiO_3$, with grain size of 89 and 97 nm, respectively. Crystallization occurrence is accompanied by Young's modulus increase from 90.92 to 98.38 GPa. On the other hand, partially crystallized samples (850°C) exhibit higher Vickers hardness (718.8) compared to fully crystallized ones (619.8), which show lower density (98.6%). *In-vitro* tests in SBF indicate that the silica-gel film preceding apatite nucleation is mostly formed on the amorphous region of substrates.

Keywords: Bioactive glasses; Spark Plasma Sintering; Rietveld method; Mechanical properties; *In-vitro* tests

1. Introduction

Owing to their ability to stimulate bone regeneration when interfaced with biological tissues and fluids, bioactive glasses are currently employed in several medical applications **[1-8]**. So far, standard 45S5 Bioglass®, originally developed by Hench and co-workers in the late sixties, has played a prominent role in this context **[7]**. In spite of this, negative features are encountered using such glass for obtaining bulk templates for bone regeneration, mostly related to its rapid tendency to crystallize at relatively low temperature values of about 600°C, when the corresponding powders are subjected to the required heat treatments **[2,9-10]**. Indeed, a reduced bioactivity is generally displayed by the resulting crystallized sintered products. To overcome this drawback, alternative glass formulations able to guarantee, on the one hand, lower tendency to crystallize, and, on the other, similar or higher bioactivity properties with respect to 45S5 Bioglass®, have been proposed in the literature **[11-17]**. They include a CaO-rich glass generally referred to as BG_Ca/Mix **[11-12,14]**, which is characterized by the following composition: 2.3% Na_2O, 2.3% K_2O, 45.6% CaO, 2.6% P_2O_5, and 47.2% SiO_2 (mol. %). More recently, the introduction of strontium and magnesium, which are known to provide beneficial (therapeutic) effects **[18-20]** in bioactive glass (BG), was explored to generate the so called BGMS10 **[13,15],** Bio_MS **[16]** and BGMSN **[17]** formulations. These three glasses were specifically designed to achieve very high crystallization temperatures, in order to avoid crystallization phenomena upon thermal treatments; on the other hand, such thermal treatments are necessary to fabricate sintered bodies, coatings, scaffolds, etc. To preserve the low crystallization peculiarity, a high content of CaO was kept in these glasses, i.e. 25.6 mol.% for BGMS10 and 31.3 mol.% for Bio_MS and BGMSN, respectively. BGMS10, Bio_MS and BGMSN displayed crystallization temperatures

among the highest ever reported in the literature (932 °C, 859 °C and 851 °C, respectively), and, at the same time, outstanding properties in terms of bioactivity and biocompatibility, which were tested also with an innovative 3D cellular model **[15-16]**. Such model mimicked the potential clinical application of the materials and employed human bone marrow mesenchymal stem cells. Furthermore, the reactivity and dissolution behaviour of such products was confirmed by means of a Molecular Dynamics model **[21]**. Thus, such bioactive glasses showed a very favourable combination of properties, i.e. an excellent biological performance and a very high crystallization temperature at the same time. Therefore, these BGs could be considered very promising for bone tissue engineering and regenerative medicine, particularly when a thermal treatment is necessary to produce a specific device.

Once the nominal composition of the glass is set, it is very important to achieve the most suitable microstructural characteristics, so that both the bioactivity and the mechanical properties of the corresponding sintered products are optimized. Since both these characteristics depend on sample porosity (volume percentage, pores size and distribution), the latter one should be maintained the same when the effect produced by other structural parameters, for instance the crystallization level attained during sintering, has to be proved. Unfortunately, such condition is quite difficult to achieve.

To overcome this obstacle, a preliminarily comparison of mechanical and biological behavior could be assessed by considering fully dense glass-derived products, so that possible masked effects induced by other difficult-to-control parameters associated to porous bodies are avoided. A strong support in this regard could be provided by the use of Spark Plasma Sintering (SPS) for powder consolidation. Indeed, due to its intrinsic peculiarities, SPS is not only very efficient and typically permits to obtain dense

products in relatively shorter times/milder temperatures compared to conventional sintering methods, but also allows to carefully control processing parameters for hindering devitrification phenomena from the parent glass or obtaining desirable crystallization levels. All these advantages were recently exploited to produce nearly full dense 45S5 **[22]** and BG_Ca/Mix **[14]** glass samples as well as composites **[23]**, with different crystallinity degree and evaluate their behavior during biological tests in SBF (Simulated Body Fluid).

The present investigation is first aimed to identify the optimal temperature conditions to fully consolidate BGMS10 powders by SPS. Three sets of dense sintered products with diverse crystallinity ratio are then obtained for further characterization. A detailed microstructural analysis is carried out to quantitatively estimate crystallinity ratio, phases content, and crystallite size. Finally, their mechanical and biological properties are evaluated and compared.

2. Experimental Materials and Methods

2.1 Powders

The nominal chemical composition (mol%) of the lab-made BGMS10 bioactive glass powders investigated in this work is: 2.3% Na_2O, 2.3% K_2O, 25.6% CaO, 10.0% MgO, 10.0% SrO, 2.6% P_2O_5, and 47.2% SiO_2. The preparation of glass powders is described in detail elsewhere **[13]**.

Particle size distribution was determined by laser light scattering analyser (CILAS 1180, France). The powders' morphology was examined by high-resolution scanning electron microscopy (HR-SEM, mod. S4000, Hitachi, Tokyo, Japan). The density of BGMS10 was measured by means of a gas pycnometer (Accupyc II 1340, Micromeritics USA), which provided a value of 2.97 g/cm^3. To assess the thermal behavior of glass powders, differential thermal analysis (DTA) (Netzsch Differential Thermal Analyzer, DSC 404, Netzsch-Gerätebau GmbH, Selb, Germany) was carried out from room temperature to 1000°C under air flow. The corresponding data obtained at different heating rates, in the range 8-30 °C/min, were also used to estimate the effective activation energy of the crystallization process ($\boldsymbol{E_c}$), according to the Kissinger theory **[24]** using the following expression

$$\ln\left(\frac{r}{T_p^2}\right) = -\frac{E_c}{RT_p} + C \qquad (1)$$

where $\boldsymbol{T_p}$(K) is the temperature value relative to the exothermic peak in the DTA curve, $\boldsymbol{r}$ the heating rate, and $\boldsymbol{R}$ the universal gas constant.

2.2 Bulk samples

Cylindrical samples of about 15 mm diameter and 3 mm thickness were produced from BGMS10 powders using a SPS apparatus (515S model, Fuji Electronic Industrial Co., Ltd., Kanagawa, Japan). Sintering experiments were carried out in vacuum (about 20 Pa), using a current sequence of 12 ON pulses followed by 2 OFF pulses, and 3.3 ms as characteristic time of single pulse. Temperature was measured using a K-type thermocouple (Omega Engineering Inc., USA) inserted in a small hole drilled on the external surface of graphite dies. Bulk BGMS10-derived samples were prepared at different dwell temperature conditions (T_D), in the range 650-950°C, whereas holding time (t_D) and mechanical pressure (P) were kept constant equal to 2 min and 16 MPa, respectively. During SPS, the temperature was first increased at a rate of 50°C/min from the ambient value to 100°C below T_D. Heating rate was then lowered (10°C/min), to minimize overshooting problems, until the dwell temperature was achieved. For the sake of reproducibility, each experimental run was replicated at least twice.

Densities of polished sintered samples were determined by the Archimedes' method using ethanol as immersing medium.

The amorphous or crystalline nature of the differently SPSed products was first assessed by X-Ray Diffraction (XRD) analysis (Smart Lab rotating anode diffractometer) using a Cu Kα radiation under the following experimental conditions: Range: 10-130°; Step: 0.05°; dwell time: 10 sec.

Phases, their amount (wt.%) and the related structural parameters were determined according to the Rietveld method, using the MAUD program **[25].**

HR-SEM was also used to examine the microstructure of the sintered specimens, after being chemically etched for time intervals up to 5 min using a 1 vol.% HF solution.

High-resolution TEM analysis was performed using a FEI TECNAI 200 operating at 200 kV working with a field emission electron gun.

Mechanical properties were assessed by micro-indentation using an Open Platform equipment (CSM Instruments, Peseux, Switzerland), with a Vickers indenter tip. Such technique was used to investigate both Young's modulus and hardness of the products. The SPSed samples, sintered at different temperatures (namely 750 °C, 850 °C and 950 °C), were embedded into epoxy resin and then lapped and polished. A maximum load of 100 mN was employed for the indentation process, with a load/unload rate of 200 mN/min. Fifteen measurements were recorded for each SPSed sample, where the load–penetration depth curve was automatically acquired for each measure. The Young's modulus was calculated from the unloading part of the load–depth curve according to **[26]**.

The *in vitro* bioactivity of samples is often investigated by soaking them in Simulated Body Fluid (SBF), according to the well-known and commonly used protocol developed by Kokubo **[27]**. Samples sintered at different temperatures were immersed in SBF solution, being the latter one and the corresponding volume used during the test prepared and calculated according to the aforementioned protocol. The samples were soaked in SBF for 3 and 7 days and stored at 37 °C in an incubator, refreshing the solution every 2 days. After each soaking time, the SPSed samples were carefully washed with distilled water and then left to dry at room temperature. Bioactivity is commonly evaluated as the ability of the material to form a surface layer of hydroxycarbonate apatite (HCA), and/or of a silica-gel film from which HCA nucleates, once in contact with physiological fluids. HCA and silica-gel formation on the surface of sintered samples was detected by means of ESEM (Quanta 2000, FEI Co., Eindhoven, The Netherlands).

3. Results and discussion

3.1 Powders

Particles size measurement of BGMS10 powders by laser light scattering gave the following values for d_{10}, d_{50}, d_{90}, and d_{av}: 0.83 ± 0.01, 4.86 ± 0.1, 26.20 ± 0.30, and 9.43 ± 0.11 μm, respectively. These data are consistent with SEM observation (**Figure 1**) which indicates that these powders consist of irregular particles with size less than about 25 μm, most of them being aggregates of few micrometers sized grains.

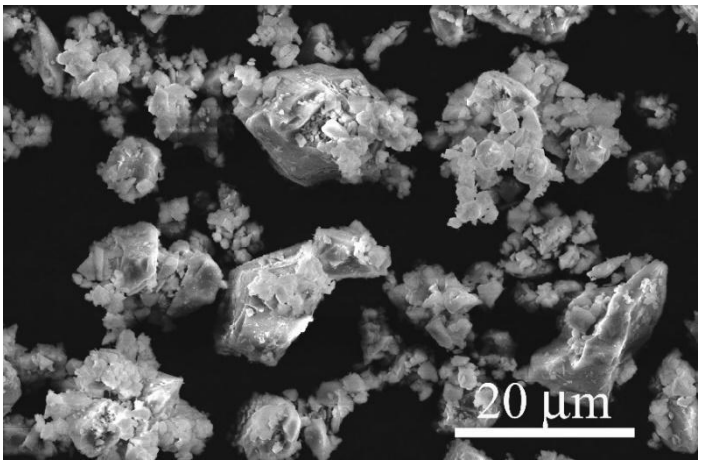

Figure 1. SEM images of the BGMS10 powders investigated in the present work.

Three representative DTA curves obtained at different heating rates are plotted in **Figure 2(a)**. The characteristic endothermic peak corresponding to the glass transition clearly shifts from about 880 to 920 °C as the test was conducted at progressively higher heating rates. As shown in **Figure 2(b)**, by plotting $\ln\left(\frac{r}{T_p^2}\right)$ as a function of $\frac{1}{T_p}$ (Kissinger plot) a straight line is obtained, according to eq. (1).

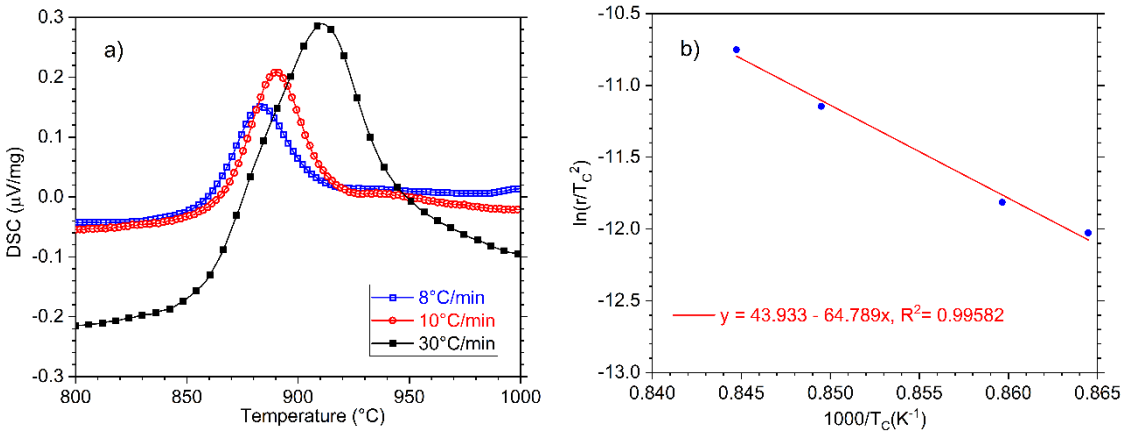

Figure 2. DTA curves (a) of BGMS10 powders at different heating rates and (b) corresponding Kissinger plot.

The estimated effective activation energy for the crystallization process is 538.9 kJ/mol. The latter value is significantly higher with respect to the range of E_c data reported in the literature for commercial Bioglass® (230-338 kJ/mol) and S53P4 (283-311 kJ/mol) glasses, also determined using the Kissinger method **[24].** On the other hand, the E_c value calculated in this work for BGMS10 is very close to that (520.8 kJ/mol) obtained for the BG_Ca/Mix bioactive glass **[12]**.

The result above provides a further indication of the markedly lower tendency to crystallize of innovative BGMS10 and BG_Ca/Mix formulations compared to standard ones.

3.2 Bulk Samples

As shown in **Figure 3(a)**, initial BGMS10 powders are white-colored. Their consolidation carried out by SPS at different holding temperatures has led to the bulk samples reported in **Figures 3(b)-3(f)**. Sintered samples processed at 650°C (**Figure 3(b)**) maintained the original powders color. Conversely, as the holding temperature is

increased from 700 to 850 °C, the resulting products changes progressively their color from light to dark-grey (**Figures 3(c)-3(e)**), respectively. Surprisingly, a further increase of the T_D value (950°C) turns the color sample to white (**Figure 3(f)**). This outcome might be correlated with the structural/compositional changes of the glass powders when processed at different conditions by SPS, as discussed afterwards.

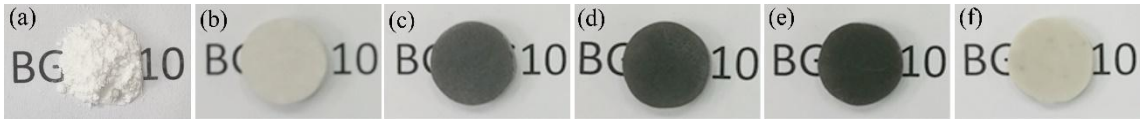

Figure 3: Images of (a) initial BGMS10 powders and the corresponding bulk samples produced by SPS at different T_D values: (b) 650°C, (c) 700°C, (d) 750°C, (e) 850°C, and (f) 950°C.

The effect of the dwell temperature on the density of SPS products is shown in **Figure 4**. The sample obtained at T_D=650°C displays an average relative density equal to about 95 %. Powder densification is progressively improved as the sintering temperature is augmented to 750°C. The absolute density value achieved in the latter case is 2.96 g/cm^3, very close to the theoretical value (99.7%). On the other hand, average relative densities of samples obtained at 850 and 950°C are slightly lower, albeit still very high, i.e. 99.3 and 98.6%, respectively.

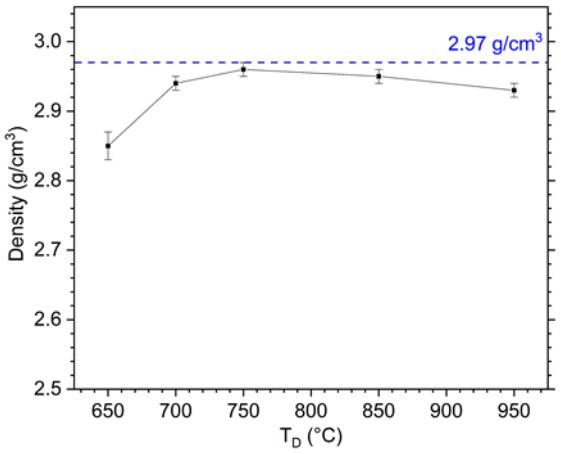

Figure 4. Influence of the holding temperature on the density of BGMS10 products obtained by SPS (t_D=2 min, P=16 MPa)

Structural and compositional characteristics of SPS samples produced in the T_D range 750-950°C are first investigated by XRD analysis (**Figure 5**). The pattern referred to the system prepared at 750 °C presents a typical shape of an amorphous glass. The phase, named as $Ca_{1.5}Na_{2.64}Si_9O_3$, has been computed using a pseudo-crystalline structure factor ($Ca_{1.5}Na_{2.64}Si_9O_3$ phase; symmetry: trigonal; space group: R-3m; crystallite size: 20 Å; microstrain: 0.03) according to the LeBail approach **[28]**.

Figure 5 also evidences that the XRD pattern of the sample sintered at 850 °C is still characterized by the halo peak ascribable to the amorphous $Ca_{1.5}Na_{2.64}Si_9O_3$. However, differently from the previous sample, some small Bragg reflections are also observed. The latter ones were then fitted with the two polymorphs of $CaSiO_3$ (α-$CaSiO_3$, Pseudowollastonite, monoclinic *C2/c* and β-$CaSiO_3$, Wollastonite, triclinic *P-1*), whose amount was estimated to be approximately equal to 1.1 and 1.0 wt.%, respectively. This aspect was further investigated by TEM. The high-magnification TEM image presented in **Figure 6(a)**, suggests that the systems prepared at 850°C presents crystalline grains dispersed into an amorphous matrix. On the other hand, as the temperature was increased

at 950 °C, the microstructure of the system shown in **Figure 6(b)**, is characterized by well-defined crystalline grains (average dimension of 900 Å) surrounded by a thin layer of amorphous nature. The Rietveld analysis of the sample prepared at 950 °C revealed that it basically consists of two crystalline phases, namely α-$CaSiO_3$ and β-$CaSiO_3$ (**Figure 5**). A third phase is represented by the halo of the amorphous glass, apparently still present at this temperature (estimated to be ~ 5 wt.%). There are some additional minor peaks at low diffraction angles, which are difficult to attribute; in any case, their presence can be considered negligible. Microstructure parameters and relative amount of each phase, estimated by Rietveld method, are reported in **Table 1**.

Bulk samples have also been examined by SEM after being chemically etched. Three representative micrographs of sintered products obtained at 750, 850, and 950 °C are shown in **Figures 7(a)-7(c)**, respectively. The resulting microstructures are quite different, with the presence of very small grains (up to 100 nm sized) observable only for the case of T_D=950°C. No further definite features could be deduced by this analysis.

The fact that, based on XRD analysis and TEM observation, devitrification phenomena already occurred in samples produced by SPS at T_D=850°C, while the crystallization temperature of BGMS10 was previously reported to be relatively higher, i.e. 932°C **[13]**, can be explained as follows. As reported in the Experimental section, during SPS, temperature is measured using a thermocouple inserted into a small orifice drilled at the center of the lateral die surface. Due to the unavoidable presence of thermal gradients across the radial direction, glass powders are very likely exposed to temperatures higher than the prescribed T_D value. Therefore, it is not surprising that the incipient crystallization was observed in SPS samples produced at T_D=850°C.

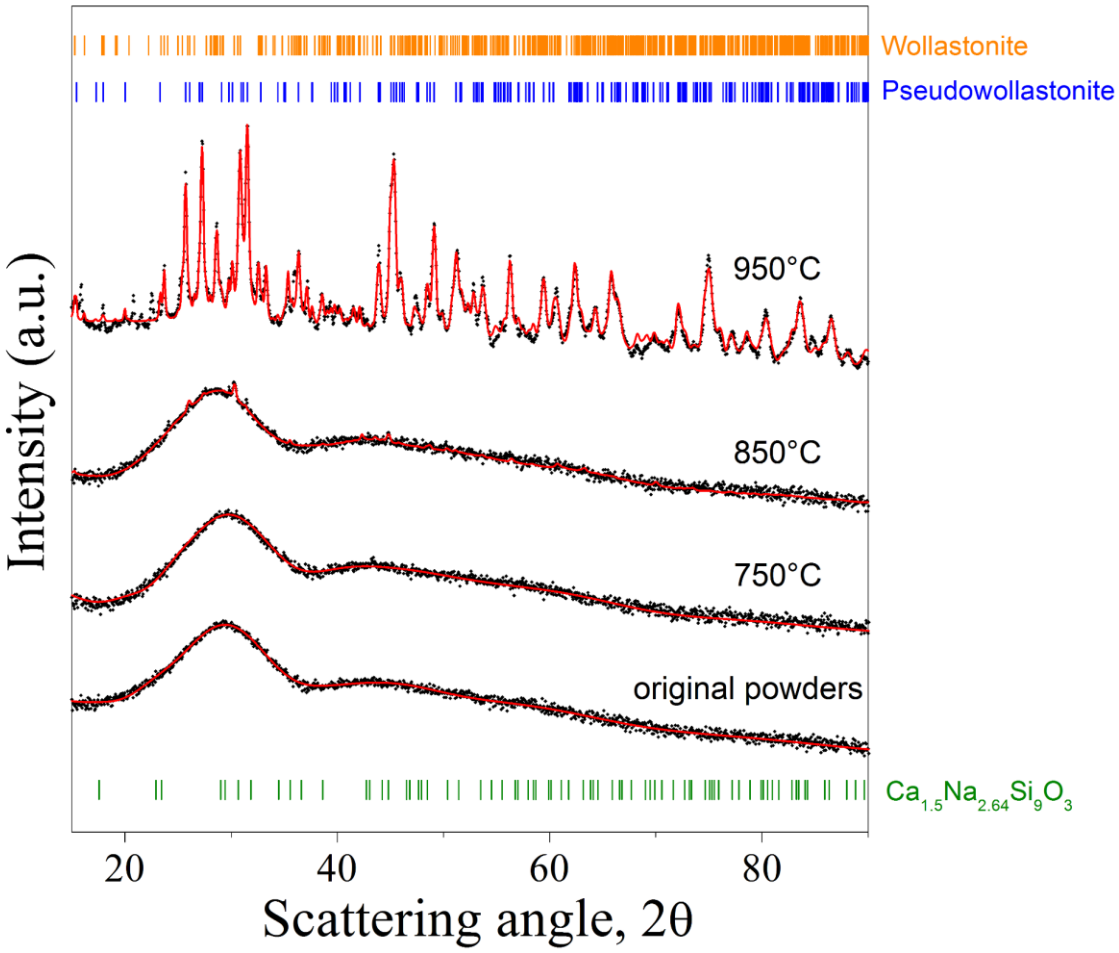

Figure 5. XRD patterns of BGMS10 samples sintered at various temperatures. Original glass powders data are also shown for the sake of comparison. Black dots are experimental data, the red line is the calculated fit. The bar sequence marks the expected peak position from the values of lattice parameters and space group of the crystallographic phases.

Table 1. Microstructural parameters and amount of each phase present on the SPS product obtained at 950°C, as estimated by the Rietveld analysis performed on the related XRD pattern (**Figure 5**). Cell volumes were calculated with the common equations for monoclinic ($V = a \cdot b \cdot c \cdot sin\,\beta$) and triclinic ($V = a \cdot b \cdot c \cdot \sqrt{(1 - coscos2 \cdot \alpha - cos\,cos\,2 \cdot \beta - cos\,cos\,2 \cdot \gamma + 2\,cos\,cos\,\alpha\,cos\,cos\,\beta\,cos\,cos\,\gamma)}$) cells.

Phase	**Space group**	**a (Å)**	**b (Å)**	**c (Å)**	**Angle (°)**	**V (Å³)**	**Cryst. size (Å)**	**R.m.s strain**	**Content (wt.%)**	**Rwp (%)**
Pseudowollastonite	Mono (*C2/c*)	6.9269	12.0051	19.7794	β = 90	1644.82	887	$1.5*10^{-3}$	59	9.67
Wollastonite	Triclinic (*P-1*)	7.8557	7.0647	7.1579	α = 89.5 β = 95.6 γ = 103.1	385.03	968	$1.7*10^{-3}$	36	
$Ca_{1.5}Na_{2.64}Si_9O_3$ (amorphous phase)	Trigonal (*R-3m*)	-	-	-	-	-	-	-	5	

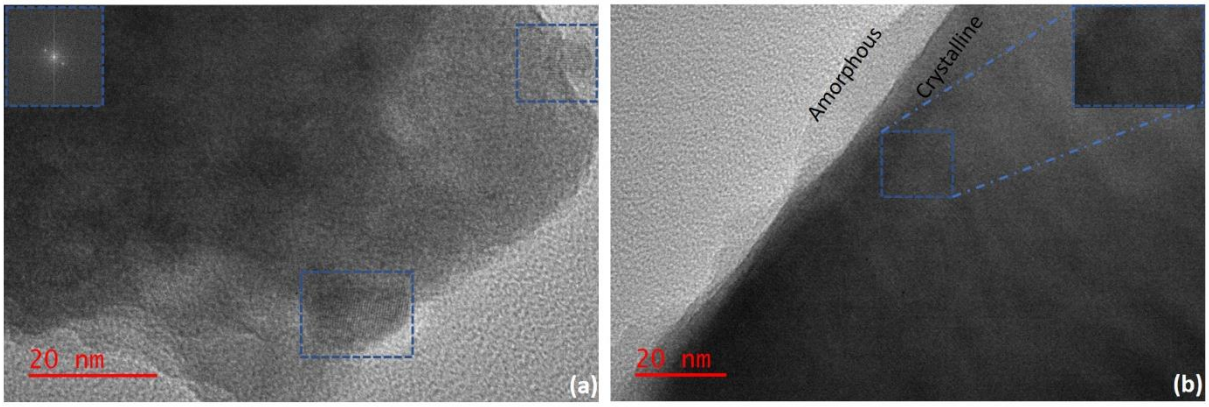

Figure 6. Representative HR-TEM images of the samples treated at (a) 850 °C and (b) 950 °C. Fast Fourier transform (FFT) of the crystalline grains (marked by blue squares), is displayed in the inset of the left side image. A zoom of crystalline plane is marked by blue square in the right-side image.

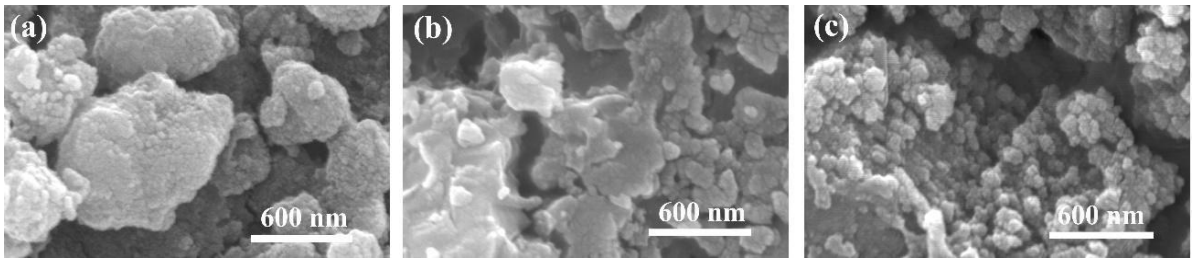

Figure 7. SEM micrographs of chemically etched dense BGMS10 products obtained by SPS (2 min/16MPa) at different sintering temperatures: (a) 750°C, (b) 850°C, and (c) 950°C.

3.3 Mechanical properties

The mechanical properties of the SPSed samples, sintered at different temperatures (namely 750, 850 and 950 °C), were investigated by the microindentation technique.

The obtained results are reported in **Table 2**.

Table 2. Mechanical properties of the SPSed samples, sintered at different temperatures

T_D [°C]	Hardness [Vickers] (mean ± standard deviation)	Young's modulus [GPa] (mean ± standard deviation)
750	671.7 ± 16.6	90.92 ± 3.42
850	718.8 ± 29.4	92.80 ± 2.22
950	619.2 ± 47.1	98.38 ± 5.90

It is worth noting that increasing the sintering temperature results in an increase in the Young's modulus. This can be ascribed to the crystallization which is achieved in samples sintered at 850 and 950 °C. Usually, crystalline materials are mechanically stronger than the amorphous counterparts **[29]**. In fact, XRD analysis evidenced that BGMS10 sintered at 750 °C was amorphous, while the sample at 850 °C was partially crystallized and that at 950 °C nearly fully crystallized (as shown in Figure 5 and Table 1). In particular, the increase of the Young's modulus from 750 °C to 950 °C can be justified by the presence of wollastonite, which is known to display good mechanical properties **[30]**.

With regard to the hardness data, the sample processed at 950 °C has a lower value compared to the other two competitors. A similar behavior was also observed by **Desogus et al. [12]** when investigating the BG_Ca/Mix system and can be explained as follows. Despite the fact the crystallization is expected to improve mechanical properties, the development of crystalline phases also implies changes in specific volumes, which may be responsible for a decrease in compactness and relative density. As a matter of fact, the density of BGMS10 samples sintered at 750 and 850 °C was very close to the theoretical value (99.7 and 99.3 %, respectively). On the other hand, samples sintered at 950°C

displayed lower values, namely 98.6%. So, the negative effect of the density reduction counterbalances the positive effect of the crystallization.

With reference to other BGs prepared by SPS, it is worth noting that the values of elastic modulus of BGMS10 samples are higher compared to those obtained with 45S5, all sintered using the same SPS technique **[12]**. The increase of mechanical properties could be explained with the beneficial contribution of MgO and SrO in the BGMS10 composition, because of their high metal-oxygen bond strength. This confirms that the presence of MgO and SrO in the BGMS10 formulation favors not only biological properties but also mechanical ones. With regard to BG_Ca/Mix SPSed samples investigated in a previous work **[12]**, the Young's modulus of BGMS10 specimens is relatively higher, i.e. about 91 instead of 65 GPa, when considering amorphous products. On the other hand, the opposite situation is encountered when considering crystallized samples. Indeed, the Young's modulus of BGMS10 product sintered in this work at 950°C equals to approximately 98.4 GPa, whereas mainly crystallized BG_Ca/Mix specimens consolidated at 850°C exhibited an average value of about 120 GPa **[12]**.

Anyways, the results obtained in this study permit to affirm that good mechanical properties could be achieved due to the combination of the particular BGMS10 composition (containing also MgO and SrO) and the well sintered microstructures.

3.4 In-vitro characterization

ESEM analyses were performed on sintered samples 3 and 7 days after immersion in SBF. Figure 8 reports the micrographs of the BGMS10 SPSed samples (sintered at 750, 850 and 950 °C) after such soaking time intervals. According to **Kokubo et al. [27]**, it is possible to preliminary evaluate the bone-bonding ability of a given material by studying

the precipitation of hydroxycarbonate apatite (HCA) on the sample itself after soaking in SBF, which is an acellular solution whose ion concentration is similar to that of the human blood plasma. In fact, bioactive glasses, once implanted in the body, bond to bone via the formation of a superficial HCA layer, which mimics the mineral phase of the bone. In this context, the tendency to crystallize of bioactive glasses during thermal treatments, which are necessary to sinter them, is among the reasons that limit the use of these materials: crystallization is reported to both slow down the sintering during the thermal treatment and to inhibit the bioactivity of the material in vitro and in vivo **[31-32]**. In addition, the partial devitrification of the glass can lead to the instability of the implant once placed in the body, since the residual amorphous phase is typically more reactive and is preferentially degraded by physiological fluids **[2]**. From this point of view, the novel BGMS10 looks particularly promising thanks to its low tendency to crystallize; with regard to the in vitro assessment of bioactivity, samples treated at lower temperature, which remained almost amorphous, are expected to be more reactive in SBF than those partly (or widely) crystallized after sintering. The findings of the ESEM analysis shown in **Figure 8** were substantially consistent with this scenario. In fact, the surfaces of the SPSed samples at 750 °C (**Figure 8a** and **8d**) are characterized by several cracks, which reveal the formation and the subsequent drying of a hydrated silica gel layer; it should be stressed that the formation of such layer is among the steps which leads to the nucleation of HCA on the glass surface, as reported in the literature **[27]**.

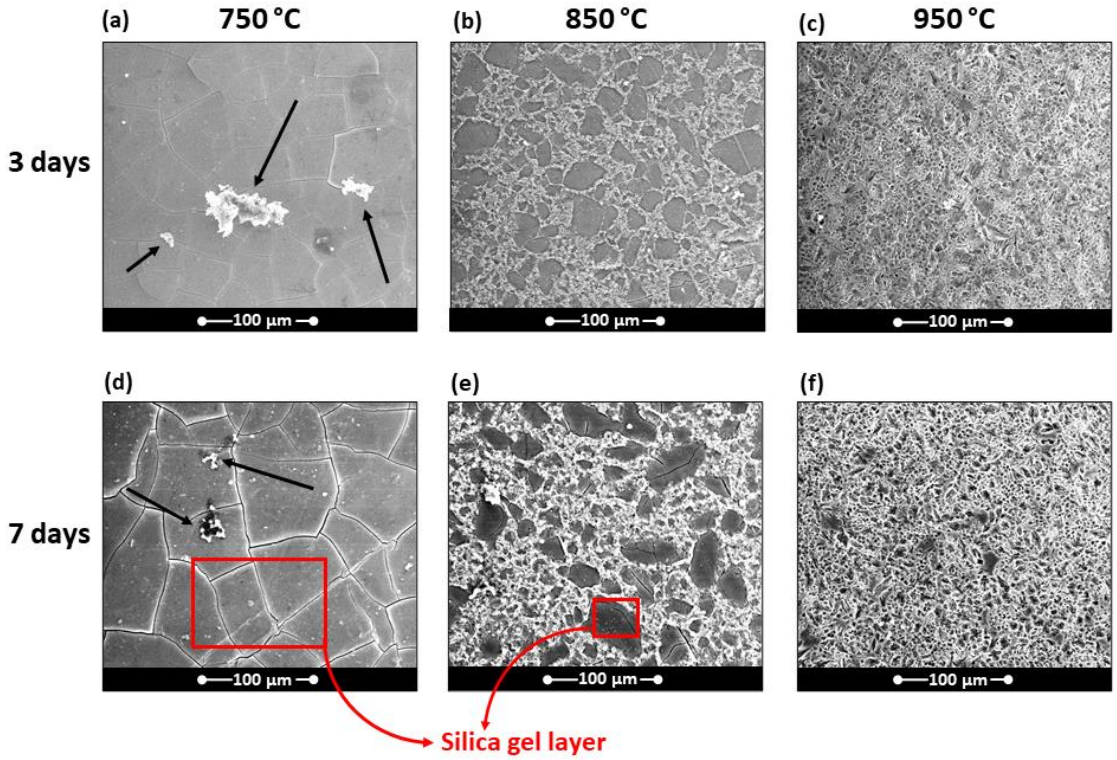

Figure 8. ESEM micrographs of the SPSed samples, sintered at different temperatures, after immersion in SBF for 3 and 7 days. Phosphorus and calcium rich precipitates are indicated by black arrows in (a) and (d).

After 7 days in SBF, the delamination of the silica gel film is even more pronounced (**Figure 8d**). Moreover, it is possible to observe the presence of phosphorus and calcium rich precipitates which locally formed on the silica gel film; the precipitation of such aggregates is a further step towards the formation an HCA layer. Conversely, the observation of the SPSed samples at 950 °C (**Figure 8c** and **8f**), which are widely crystallized, did not reveal neither the presence of the gel, nor of calcium and phosphorus rich precipitates; finally, with regard to the SPSed samples at 850 °C (**Figure 8b** and **8e**),

which are partially crystallized, it is possible to note that the formation of silica gel mainly occurs on the residual glassy areas, which appear darker in the micrographs of **Figure 8**.

Based on these observations, one should expect a better biological responsiveness for SPSed samples at 750 °C, i.e. the ones with the highest reactivity in vitro.

4. Conclusions

The aim of this work was to provide new and useful information regarding a recently developed SrO and MgO containing BGMS10 glass for possible application in the biomedical field. A main role in this study was played by the use of SPS as a powder consolidation method, which allows one to systematically investigate the effect of the sintering temperature on structural, mechanical, and biological characteristics of the obtained bulk products. Based on the obtained results, the following conclusions can be drawn:

1. the high activation energy for the crystallization process (538.9 kJ/mol), evaluated by the Kissinger formula from TGA measurements at different heating rates, confirms the very low crystallization attitude of BGMS10 glass compared to alternative formulations developed so far;
2. the optimal SPS temperature to obtain fully dense (99.7 %) products is 750°C; under the latter condition, its original amorphous nature is completely retained;
3. the incipient crystallization in the glass is revealed by XRD and TEM analyses in samples sintered at 850°C, while almost completely crystallized ceramics (95 wt. %) are produced at 950°C; α-$CaSiO_3$, and β-$CaSiO_3$ with grain size of 89 and 97 nm, respectively, are formed; a decrease in sample density is

observed in the 750-950°C range, as a consequence of crystallization occurrence;

4. as for mechanical properties, the Young's modulus is progressively improved (from 90.92 to 98.38 GPa) if crystallization in the glass takes place; on the other hand, the maximum Vickers hardness (718.8 ± 29.4) is obtained when considering partially crystallized samples (T_D=850°C) instead of the almost fully crystallized ones (T_D=950°C); this outcome is justified by the corresponding density decrease;
5. biological tests in SBF clearly evidence that the formation of the silica-gel film preceding apatite nucleation is strongly promoted by the presence of the amorphous glass on the substrate surface.

Therefore, in-vitro experiment results seem to indicate that the completely amorphous and dense BGMS10 product displays the most promising characteristics for possible biomedical applications. Such conclusion is also supported by the fact that, although improved Young's moduli are obtained in partially and fully crystallized BGMS10 samples, Vickers hardness of the amorphous counterpart is quite high and even better than that of the 95% crystallized sample. Furthermore, both these properties are much higher than those ones measured for the 45S5 Bioglass® products also processed by SPS **[12]**.

It is apparent that this study represents a first step towards the validation of BGMS10 formulation for potential clinical utilization. Reliable cellular tests should be also carried out to better evaluate the biological response of these materials. In addition, experiments using porous scaffolds, more likely desirable for practical applications, should be also taken into account in future investigations.

Acknowledgements

D.A. performed his activity in the framework of the International PhD in Innovation Sciences and Technologies at the University of Cagliari, Italy. S.G. acknowledge UNISS for the financial support received within the program “Fondo di Ateneo per la ricerca 2020”. All authors acknowledge the CeSAR (Centro Servizi d’Ateneo per la Ricerca) of the University of Sassari for the X-ray diffraction and TEM investigations. A.I. has been supported by a PhD program, MIUR special scholarship, within the joint agreement UNICA-UNISS for the PhD program in Chemical and Technological in Sciences.

References

[1] L.C. Gerhardt, A.R. Boccaccini, Bioactive Glass and Glass-Ceramic Scaffolds for Bone Tissue Engineering, Materials 3, (2010), 3867. https://doi.org/10.3390/ma3073867

[2] J.R. Jones Review of bioactive glass: from Hench to hybrids. Acta Biomater. 9, (2013) pp. 4457-4486. https://doi.org/10.1016/j.actbio.2012.08.023

[3] V. Miguez-Pacheco, L.L. Hench, A.R. Boccaccini, Bioactive glasses beyond bone and teeth: Emerging applications in contact with soft tissues. Acta Biomater., 13, (2015), pp. 1–15. https://doi.org/10.1016/j.actbio.2014.11.004

[4] Q. Chen, J.A. Roether, A. R. Boccaccini, Tissue Engineering Scaffolds from Bioactive Glass and Composite Materials. Top. Tissue Eng. 4, (2008), pp. 1–27. https://doi.org/10.1586/17434440.2.3.303

[5] J.R. Jones, D.S. Brauer, L. Hupa, D.C. Greenspan, Bioglass and Bioactive Glasses and Their Impact on Healthcare. Int. J. Appl. Glas. Sci. 7, (2016), pp. 423–434, https://doi.org/10.1111/ijag.12252

[6] L.L. Hench, J.M. Polak, Third-generation biomedical materials. Science, 295 (2002), pp. 1014–1017. https://doi.org/10.1126/science.1067404

[7] L.L. Hench, The story of Bioglass®, J Mater Sci – Mater Med, 17 (2006), pp. 967-978. https://doi.org/10.1007/s10856-006-0432-z

[8] F. Baino, G. Novajra, V. Miguez-Pacheco, A.R. Boccaccini, C. Vitale-Brovarone, Bioactive glasses: Special applications outside the skeletal system. J. Non. Cryst. Solids, 432 (2016), pp. 15–30. https://doi.org/10.1016/j.jnoncrysol.2015.02.015

[9] S. Grasso, R.K. Chinnam, H. Porwal, A.R. Boccaccini, M.J. Reece, Low temperature spark plasma sintering of 45S5 Bioglass®, J. Non-Cryst. Solids. 362, (2013), pp. 25-29. https://doi.org/10.1016/j.jnoncrysol.2012.11.009

[10] C. Blaeß, R. Müller, G. Poologasundarampillai, D.S. Brauer, Sintering and concomitant crystallization of bioactive glasses. Int. J. Appl. Glass Sci. 10(4), (2019), pp. 449-462. https://doi.org/10.1111/ijag.13477

[11] D. Bellucci, A. Sola, V. Cannillo, Low temperature sintering of innovative bioactive glasses, J. Am. Ceram. Soc. 95(4), (2012), pp. 1313–1319. https://doi.org/10.1111/j.1551-2916.2012.05100.x

[12] L., Desogus, A. Cuccu, S. Montinaro, G. Cao, D. Bellucci, A. Sola, V. Cannillo, Classical Bioglass® and innovative CaO-rich bioglass powders processed by Spark Plasma Sintering: A comparative study. J. Europ. Cer. Soc. 5(15), (2015) pp. 4277-4285. https://doi.org/10.1016/j.jeurceramsoc.2015.07.023

[13] D. Bellucci, V. Cannillo, A novel bioactive glass containing strontium and magnesium with ultra-high crystallization temperature, Mater. Lett. 213, (2018), pp. 67-70. https://dx.doi.org/10.1016/j.matlet.2017.11.020

[14] S. Montinaro, M. Luginina, S. Garroni, R. Orrù, F. Delogu, D. Bellucci, V. Cannillo, G. Cao, Spark Plasma Sintered CaO-rich Bioglass-derived Glass-Ceramics: a Detailed Investigation of their Behaviour during Biological Tests in SBF. J. Eur. Ceram. Soc. 39(4), (2019), pp. 1603-1612. https://dx.doi.org/10.1016/j.jeurceramsoc.2018.12.003

[15] D. Bellucci, E. Veronesi, V. Strusi, T. Petrachi, A. Murgia, I. Mastrolia, M. Dominici, V. Cannillo, Human mesenchymal stem cell combined with a new

strontium-enriched bioactive glass: an *ex-vivo* model for bone regeneration, Materials, 12(21), (2019) 3633. https://dx.doi.org/10.3390/ma12213633

[16] D. Bellucci, E. Veronesi, M. Dominici, V. Cannillo, A new bioactive glass with extremely high crystallization temperature and outstanding biological performance, Mater. Sci. Eng. C, 110, (2020) 110699. https://dx.doi.org/10.1016/j.msec.2020.110699

[17] R. Sergi, D. Bellucci, R. Salvatori, A. Anesi, V. Cannillo, A novel bioactive glass containing therapeutic ions with enhanced biocompatibility, Materials, 13(20), (2020), pp. 1–16. https://dx.doi.org/10.3390/ma13204600

[18] D. Bellucci, A. Sola, R. Salvatori, A. Anesi, L. Chiarini, V. Cannillo, Role of magnesium oxide and strontium oxide as modifiers in silicate-based bioactive glasses: Effects on thermal behaviour, mechanical properties and in-vitro bioactivity, Mater. Sci. Eng. C, 72, (2017) pp. 566–575. https://doi.org/10.1016/j.msec.2016.11.110

[19] T. Mehrabi, A.S. Mesgar, Z. Mohammadi, Bioactive Glasses: A Promising Therapeutic Ion Release Strategy for Enhancing Wound Healing. ACS Biomater. Sci. Eng. 6(10), (2020), pp. 5399-5430. https://doi.org/10.1021/acsbiomaterials.0c00528

[20] A. Hoppe, N.S. Güldal, A.R. Boccaccini, A review of the biological response to ionic dissolution products from bioactive glasses and glass-ceramics. Biomaterials, 32, (2011), pp. 2757–2774. https://doi.org/10.1016/j.biomaterials.2011.01.004

[21] A. Pedone, V. Cannillo, M.C. Menziani, Toward the understanding of crystallization, mechanical properties and reactivity of multicomponent bioactive

glasses, Acta Mater., 213, (2021), 116977. https://doi.org/10.1016/j.actamat.2021.116977

[22] S. Montinaro, L. Desogus, R. Orrù, S. Garroni, F. Delogu, P. C. Ricci, G. Cao, A Comprehensive Study on Compositional and Structural changes in 45S5 Bioglass products exposed to Simulated Body Fluid. J. Am. Ceram. Soc. 101(1), (2018), pp. 116-130. https://doi.org/10.1111/jace.15199

[23] M. Luginina, D. Angioni, S. Montinaro, R. Orrù, G. Cao, R. Sergi, D. Bellucci, V. Cannillo, Hydroxyapatite/bioactive glass functionally graded materials (FGM) for bone tissue engineering, J. Europ. Cer. Soc. 40, (2020), pp. 4623-4634. https://doi.org/10.1016/j.jeurceramsoc.2020.05.061

[24] J. Massera, S. Fagerlund, L. Hupa, M. Hupa, Crystallization mechanism of the bioactive glasses, 45S5 and S53P4. J. Am. Ceram. Soc. 95(2) (2012), pp. 607-613. https://doi.org/10.1111/j.1551-2916.2011.05012.x

[25] L. Lutterotti, R. Ceccato, R. Dal Maschio, E. Pagani, Quantitative analysis of silicate glass in ceramic materials by the Rietveld method. Mater. Sci. Forum, 87, (1998), pp. 278-281. https://doi.org/10.4028/www.scientific.net/MSF.278-281.87

[26] W. Oliver, G. Pharr, An improved technique for determining hardness and elastic modulus using load and displacement sensing indentation experiments. J. Mater. Res., 7, (1992), pp. 1564–1583. https://doi.org/10.1557/JMR.1992.1564

[27] T. Kokubo, H. Takadama, How useful is SBF in predicting in vivo bone bioactivity? Biomaterials, 27, (2006), pp. 2907–2915. https://doi.org/10.1016/j.biomaterials.2006.01.017

[28] M. Baricco, T.A. Baser, S. Enzo, G. Vaughan, A.R. Yavari, Analysis of crystallization behavior of $Fe_{48}Cr_{15}Mo_{14}Y_2C_{15}B_6$ bulk metallic glass by synchrotron

radiation. J. Mater. Res., 23, (2008), pp. 2166-2173. https://dx.doi.org/10.1557/JMR.2008.0264

[29] D. Bellucci, V. Cannillo, A. Sola, An overview of the effects of thermal processing on bioactive glasses, Sci. Sin. 42, (2010), pp. 307–320. https://doi.org/10.2298/SOS1003307B

[30] S. Kunjalukkal Padmanabhan, F. Gervaso, M. Carrozzo, F. Scalera, A. Sannino, A. Licciulli, Wollastonite/hydroxyapatite scaffolds with improved mechanical, bioactive and biodegradable properties for bone tissue engineering, Ceram. Int., 39, (2013), pp. 619–627. https://doi.org/10.1016/j.ceramint.2012.06.073

[31] A.R. Boccaccini, Q. Chen, L. Lefebvre, L. Gremillard, J. Chevalier, Sintering, crystallization and biodegradation behaviour of bioglass®-derived glass–ceramics, Faraday Discuss. 136, (2007), pp. 27–44. https://doi.org/10.1039/b616539g

[32] O. Bretcanu, X. Chatzistavrou, K. Paraskevopoulos, R. Conradt, I. Thompson, A.R. Boccaccini, Sintering and crystallization of 45S5 bioglass® powder, J. Eur. Ceram. Soc. 29, (2009), pp. 3299–3306. https://doi.org/10.1016/j.jeurceramsoc.2009.06.035